Pages: 23-33 / Vol. 17- No.1/Winter- Spring 2024

Journal of Aerospace Science and Technology

Journal homepage: www:jast.ias.ir

Original Research Article

Ionospheric electron density reconstruction over central Europe using neural networks: A comparative study

Seyyed Reza Ghaffari-Razin[1]*, Reza Davari Majd, Behzad Voosoghi, Navid Hooshangi

1-3- Department of Geoscience Engineering, Arak University of Technology, Arak, Iran
2- Department of Civil engineering, Islamic Azad University of Khoy, Khoy, Iran
4- Department of Geodesy & Geomatics Engineering, K. N. Toosi University of Technology, Tehran, Iran

ABSTRACT

Article History:
Received: 27.May.2019
Revised: 01.October.2023
Accepted: 17.October.2023
Available online: 01.June.2024

Keywords: *Total Electron Content, Tomography, Residual Minimization Training Neural Network, Ionospheric Tomography based on the Neural Network, GPS.*

DOI : doi.org/10.22034/jast.2023.187660.1020

Computerized Ionospheric Tomography (CIT) is a method to reconstruct ionospheric electron density images by computing Total Electron Content (TEC) values from the recorded GPS signals. Due to the poor spatial distribution of GPS stations, limitations of signal viewing angle, and discontinuity of observations in the time and space domain, CIT is an inverse ill-posed problem. To solve these problems, two new methods are developed and compared with the initial method of Residual Minimization Training Neural Network (RMTNN). Modified RMTNN (MRMTNN) and Ionospheric Tomography based on the Neural Network (ITNN) are considered new methods of CIT. In all two methods, Empirical Orthogonal Functions (EOFs) are used to improve the accuracy of the vertical domain. Also, Back Propagation (BP) and Particle Swarm Optimization (PSO) algorithms are used to train the neural networks. To apply the methods for constructing a 3D image of the electron density, 23 GPS measurements of the International GNSS Service (IGS) with different geomagnetic indexes are used. To validate and better assess the reliability of the proposed methods, 4 ionosondee stations have been used. Also, the results of the proposed methods have been compared to those of the NeQuick empirical ionosphere model. Based on the analysis and comparisons, the RMSE of the ITNN model at high geomagnetic activity in DOUR, JULI, PRUH, and WARS ionsonde stations are 1.22, 1.46, 1.18 and 1.19 (1011 ele./m3), respectively. The results show that the RMSE of the ITNN model is less than other models in both high and low geomagnetic activities and ionosonde stations.

Introduction

In the last two decades, the knowledge of the distribution of ionospheric electron density has been considered a major challenge for geodesy and geophysics researchers. To study the physical properties of the ionosphere, Computerized Ionospheric Tomography (CIT) indicated an efficient and effective manner. Usually, the value of Total Electron Content (TEC) is used as an input parameter to CIT. Then inversion methods are used to compute electron density at any time and space. However, CIT is considered an inverse ill-posed problem due to the lack of input observations and non-uniform distribution of TEC data. The ionosphere has temporal and spatial variations. Also, it has daily, monthly, and yearly frequencies. Due to the different time frequencies, ionosphere analysis is extremely important. The ionosphere has major importance to us because, among other functions, it influences radio

1 *Corresponding Author, Seyyed Reza Ghaffari-Razin , Assistan Professor , Email: mr.ghafari@arakut.ac.ir

Print ISSN:1735-2134 Online ISSN: 2345-3648

propagation to distant places on the earth, and between satellites and earth. The ionosphere plays an important role in space science, radio communication, and satellite positioning. During the solar activity periods, it has many variations and fluctuations. Therefore, it is very important to know how the electron density is distributed as a function of time and space.

Many algorithms and methods are presented to model CIT. For the first time, 2-dimensional CIT was suggested by [1]. They used Algebraic Reconstruction Techniques (ART) to obtain the electron density. Kunitsyn et al. (2011) used ionospheric radio tomography based on data from high-orbital navigation systems [2]. The minimum Sobolev's norm was suggested for finding the solution. Pokhotelov et al. (2011) used 4D tomography reconstruction to detect ionosphere anomalies in the high-latitude polar cap region [3]. Wen et al. (2012) presented a new tomographic algorithm, termed Two-Step Algorithm (TSA). In this method, the electron density is estimated in two steps; the Phillips Smoothing Method (PSM) is used to resolve the ill-conditioned problem, and the PSM solution is input as an initial value to the algebraic reconstruction technique [4]. Van de Kamp (2013) examined the ionosphere above Scandinavia by 4-dimensional tomography using the software package MIDAS from the University of Bath [5]. Ghaffari Razin (2015) expanded 3D ionosphere tomography by combining spherical harmonics and empirical orthogonal functions. The zero-order Tikhonov regularization is used for parameter estimations [6]. Ghaffari Razin and Voosoghi (2016) developed a local ionosphere tomography model over Iran using SCHs [7]. Although the results of all studies indicate the high efficiency of CIT, two major limitations can be considered to this method: first, due to poor spatial distribution of Global Positioning System (GPS) stations and limitations of signal viewing angle, CIT is an inverse ill-posed problem. Second, in most cases, observations are discontinuous in the time and space domain, so the density profiles can't be at any time and space around the world.

Artificial Neural Networks (ANNs) are one of the new ideas to solve the mentioned problems. ANNs are a set of information processing systems that have been formed by simple processing elements called artificial neurons. Methods of artificial intelligence provide a valuable tool that makes it possible to model the nonlinear behavior of the ionosphere [8]. Ma et al., (2005) demonstrated the idea of using aNNs to solve the ipheric tomography [9]. They used Standard ANNs (SANNs) with a Back-Propagation (BP) algorithm to train the network. Also used ionosondee observations to improve the vertical resolution. After that, Hirooka et al., (2011) used the same ANNs to model the ionospheric electron density distributions [10]. They used Low Earth Orbit (LEO) observations as vertical constraints and updated neural weights using these pieces of information. Low accuracy in the vertical domain is a major disadvantage of these two studies. To solve the low accuracy in the vertical domain, Ghaffari Razin and Voosoghi (2016) used Empirical Orthogonal Functions (EOFs) as vertical constraints [11]. Using EOFs improved the accuracy of the vertical domain but accuracy in the time domain remains a major challenge.

The goal of this paper is to improve CIT modeling using Neural Networks (NNs). Two methods of ionospheric tomography using ANNs are developed and compared. These methods include Modified Residual Minimization Training Neural Network (MRMTNN) and Ionospheric Tomography based on the Neural Network (ITNN). SANNs and Wavelet Neural Networks (WNN) have been used as base NNs. Back-propagation (BP) and Particle Swarm Optimization (PSO) algorithms are used for training these methods (MRMTNN and ITNN). The main problem in previous models is their low temporal resolution. Therefore, in this paper, the idea of using WNN along with the PSO algorithm is proposed to improve temporal resolution. Observations of 30 days in 3 different geomagnetic activity indexes (Day Of Year (DOY): 354 to 363 and 44 to 53 in 2013, 67 to 76 in 2012) are selected to apply the methods. K_p values less than 3 ($K_P < 3$) are considered as the quiet day, K_p values between 3 and 5 are considered as the medium condition, and K_p values greater than 5 are considered as the stormy days. The accuracy of the results is controlled with 4 ionosondee stations. At the ionosondee stations, the accuracy of the reconstructed electron density is evaluated. Also, all the results have been compared with the NeQuick empirical ionosphere model.

Data and input observations

The pixel-based tomographic reconstruction is implemented by using IGS data from 23 Global Navigation Satellite System (GNSS) stations (as

shown in Figure 1) for 3 periods with different geomagnetic activity (354 to 363 in 2013, 44 to 53 in 2013, 67 to 76 at 2012). Receiver Independent Exchange format (RINEX) observation files with a sampling rate of 30 seconds have been downloaded from the Crustal Dynamics Data Information System (CDDIS) as a global data center of IGS [12]. The results are compared with the electron density derived from ionosondee data [13] and the NeQuick empirical model of electron density. As shown in Figure 1, 4 ionosondee stations DOUR (50.10^{0}N, 4.60^{0}E), JULI (54.60^{0}N, 13.40^{0}E), PRUH (50.00^{0}N, 14.60^{0}E), WARS (52.20^{0}N, 21.20^{0}E) are located in the research area. So there is the possibility of a more accurate evaluation of the three proposed methods.

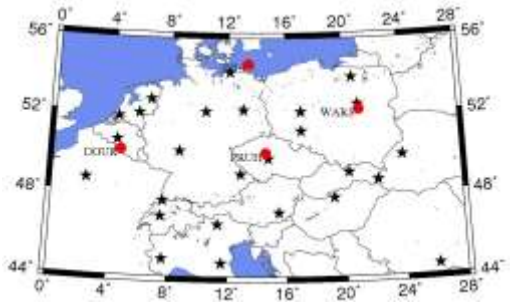

Fig. 1. Distribution of GPS stations (black stars) and ionosondee stations (red circles).

The spatial resolution along the longitude, latitude, and altitude is considered 0.5^0×0.5^0×30 (km). Thus, the total number of voxels is 40320. Using data from space weather prediction centers, these days have different geomagnetic activity indices. In Figure 2, the green bars indicate K_p values less than 3 ($K_P < 3$), the yellow bars show K_p values greater than 3 ($5 \geq K_P \geq 3$), and the red bar demonstrates K_p values greater than 5 ($K_P > 5$). In all of the processing, DOY from 354 to 363, 44 to 53, and 67 to 76 are considered as the quiet days, medium condition, and stormy days, respectively.

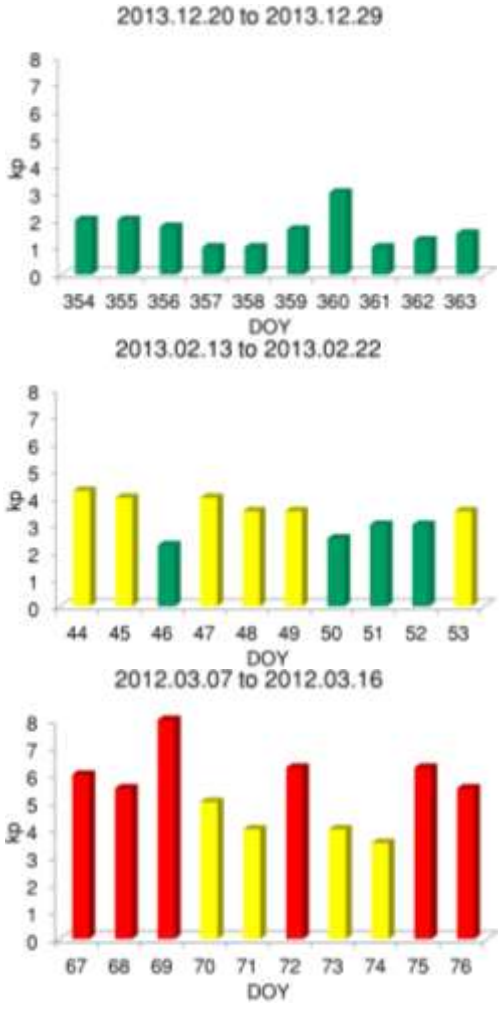

Fig. 2. Kp index for 3 observation periods.

Using ground-based GPS receivers, it is possible to compute Slant TEC (STEC). That is one of the most important data sources in ionospheric research. Carrier phase-derived STEC ($STEC_L$) and code pseudo-ranges STEC ($STEC_P$) are calculated with the following equations [14]:

$$STEC_L = \frac{(f_1 f_2)^2}{40.3(f_1^2 - f_2^2)}(L_1\lambda_1 - L_2\lambda_2) \quad (1)$$

$$STEC_P = \frac{(f_1 f_2)^2}{40.3(f_1^2 - f_2^2)}(P_2 - P_1) \quad (2)$$

where $f_1$and $f_2$are signal frequency, $L_1$and $L_2$are the carrier phase measurements, λ_1 and λ_2 are the wavelengths, P_1 and $P_2$are the code pseudo-ranges measurements. Carrier phase-derived $STEC_L$ depends on the ambiguity parameters while the code derived $STEC_P$observation is noisy. To reduce the multipath and noise level in the $STEC_P$, the carrier phase measurements are used to compute a more precise relative STEC observable. In this approach, the continuous arcs of $STEC_L$are adjusted to the mean value of the corresponding

code $STEC_P$value. The mean value is computed for every continuous arc using the following equation [14]:

$$\langle STEC_P + STEC_L \rangle = \frac{1}{N}\sum_{i=1}^{N}(STEC_P + STEC_L)_i \quad (3)$$

where N is the number of continuous measurements contained in the arc. Subtracting eq. (1) from (3), the smoothed STEC can be derived [14]:

$$STEC_{smoothed} = \langle STEC_P + STEC_L \rangle - STEC_L = STEC + (B_r^P + B_s^P) + \varepsilon_{P4} \quad (4)$$

where B_r^P and B_s^P is the receiver and satellite code-delay Inter-Frequency Bias (IFB) in TECU respectively and $\varepsilon_{P4}$is the combination of multipath and measurement noise on P_1 and P_2 in TECU. The $STEC_{smoothed}$ will appear in the observation equations as the main constraints.

Modeling techniques for computerized ionospheric tomography

ANNs have been demonstrated to be a tool for the prediction of ionospheric variations (time and space dependent), which is by nature highly non-linear. A main benefit of using ANNs for the prediction of ionospheric variations over analytical methods is that no previous information on the nature of the non-linear relationships is needed. The first idea of using ANNs in ionospheric tomography was provided by [9]. They used the method described by [15] namely Residual Minimization Training Neural Network (RMTNN). In the next section, this method will be explained briefly. After introducing the details of the RMTNN method, the two new methods (MRMTNN and ITNN) presented in this paper are fully explained. The results of these two methods are compared and evaluated with the main method (RMTNN).

Residual Minimization Training Neural Network (RMTNN)

STEC as the integrated value of the ionospheric and plasmaspheric electron density can be calculated using the following equation [16]:

$$STEC_{smoothed} = \int_r^s N(\vec{r},t)ds + P_r^s \quad (5)$$

where $N(\vec{r},t)$ shows electron density at the position $\vec{r}(\phi,\lambda,h)$and observational time t, P_r^s is the contribution of the plasmaspheric electron density, r, and s indicate the total number of receivers and satellites, respectively [9]. The computational domain is divided into the ionospheric region (100 km to 1000 km) and the plasmaspheric region (above 1000 km). With discretize of Eq. (5) can be written [9]:

$$STEC_{smoothed} \approx \sum_{d=1}^{D}\beta_d N(\vec{r},t) + P_r^s \quad (6)$$

where D shows mesh points and β corresponding weight in the numerical integration. To see the role of β in numerical integration, please refer to [17]. Using Eq. (6), it can be defined the cost function of the ANN model as follows [9]:

$$C_1 = \left(\sum_{d=1}^{D}\beta_d N(\vec{r},t) + P_r^s - STEC_{smoothed}\right)^2 \quad (7)$$

The most significant drawback of ionospheric tomography is the low accuracy in the vertical domain. To compute the vertical cost function, Empirical Orthogonal Functions (*EOFs*) are used [11]. Using this method, the neural network is trained and the vertical cost function is given as [11]:

$$C_2 = \sum_{g=1}^{G}\left(N_g(h) - N_g^{EOF}\right)^2 \quad (8)$$

where G is the total number of *EOFs*, $N_g(h)$ is the output of the neural network, and $N_g^{EOF}$is the EOF_S electron density. Thus, the total cost function is considered as follows [11]:

$$C = C_1 + \gamma C_2 \quad (9)$$

where γ is the balance parameter between two cost functions. To select the value of γ, the amount of error in the cost function C is used. If the value of cost function C is below 2×10^{11} (el/m^3), the neural network is converged to the optimal result. This value has been empirically determined. As a result, $\gamma = 0.94$ is selected as the balance parameter.

Modified Residual Minimization Training Neural Network (MRMTNN)

In the RMTNN method, SANN is used. The standard sigmoid ANNs have a series of disadvantages. Typically, the initial weights of the ANNs are randomly selected in these networks. Randomly chosen initial weights of the network are increasing significantly training time. Also, when the activation function is sigmoidal type, there is always a remarkable change that the training algorithm will converge to local minima. Finally, there is no logical connection between the

activation function, optimal network structure, and the complexity of the mathematical model. Therefore, instead of using the conventional sigmoid activation functions can be used wavelet neural network. The WNN employing non-linear wavelet basis functions (named wavelets), which are localized in both the time and frequency space, has been extended as an alternative approach to the non-linear fitting problem [18]. In WNN the network output is given by the following equation [18]:

$$g_\lambda(\boldsymbol{x};\boldsymbol{w}) = \hat{y}(\boldsymbol{x}) = \omega_{\lambda+1} + \sum_{j=1}^{\lambda} \omega_j . \Psi_j(\boldsymbol{x}) + \sum_{i=1}^{n} \omega_i . x_i \quad (10)$$

In this equation, **x** is the input vector, $\Psi_j(\boldsymbol{x})$ is a multi-dimensional wavelet that is constructed by the tensor product of *m* scalar wavelets, *n* is the number of inputs, λ is the number of hidden units and ω shows a network weight. Multi-dimensional wavelets can be calculated by the following equation [18]:

$$\Psi_j(\boldsymbol{x}) = \prod_{i=1}^{m} \psi(z_{ij}) \quad (11)$$

where ψ is the mother wavelet and can be written [18]:

$$z_{ij} = \frac{x_i - a_{ij}}{b_{ij}} \quad (12)$$

In Eq. (12), $i = 1,\dots,m \quad , \quad j = 1,\dots,\lambda+1$ and the weights ω are related to the translation (a_{ij}) and the dilation (b_{ij}) parameters. The choice of the mother wavelet depends on the applications. The activation function can be considered orthogonal wavelets or continuous wavelets. In this paper, we used the Mexican hat function as a mother wavelet. This wavelet has many benefits and also has shown satisfactory results in other applications [19, 20]. The analytical form of the Mexican hat function is as follows [19]:

$$\psi(z_{ij}) = (1 - 2z_{ij}^2) e^{-\frac{1}{2}z_{ij}^2} \quad (13)$$

To optimize the initialization of the wavelet parameters, various methods have been proposed [21, 22]. The translation and dilation parameters are used as follows [23]:

$$a_{ij} = 0.5(N_i + M_i) \quad (14)$$

$$b_{ij} = 0.2(M_i - N_i) \quad (15)$$

where N_i and M_i are defined as the minimum and maximum of input $\boldsymbol{x}_i$. In the WNN, in addition to the network weights, translation and dilation parameters are updated.

Ionospheric Tomography based on the Neural Network (ITNN)

The usually used training algorithm for ANNs and WNN is the BP algorithm, which is a gradient-based method. The BP algorithm easily falls into the trap of local minima, especially for complex function approximation problems. So the BP algorithm is weak to find a global optimal solution. Also, the speed of convergence to the optimal solution is very low in this algorithm. Other key issues in this algorithm can be considered: dependence on the initial values of the weights, as well as optimal selection of the parameters such as the learning rate and the momentum. This disadvantage can be removed by an exploration ability of the swarm intelligence algorithms such as PSO. Unlike BP, PSO is a global search and population-based algorithm that has been used for training neural networks, finding neural network architectures, tuning network learning parameters, and optimizing network weights. PSO avoids trapping in a local minimum, because it is not based on gradient information. The equations used in this algorithm are considered as follows [24]:

$$v_i^{t+1} = w \times v_i^t + c_1 \times rand \times \left(pbest_i - x_i^t\right) + c_2 \times rand \times \left(gbest - x_i^t\right) \quad (16)$$

$$x_i^{t+1} = x_i^t + v_i^{t+1} \quad (17)$$

where *w* is inertia weight, v_i^t is the velocity of particle *i* at iteration *t*, c_1, and c_2 are acceleration coefficients, *rand* is a random number within [0,1], x_i^t defines the current location of particle *i* at iteration *t*, $pbest_i$ demonstrates the *pbest* of factor *i* at iteration *t*, and *gbest* is the best solution so far. In each iteration, the velocities of particles are calculated by Eq. (16). Then, the locations of particles are computed by Eq. (17). The particle positions will be varied until a stopping condition is met.

Statistical analysis

In this paper, results were analyzed based on Root Mean Square Error (RMSE), bias and correlation coefficient. These three indices are calculated as follows [25]:

$$RMSE = \sqrt{\frac{1}{M}\sum_{i=1}^{M}\left(N_R^i - N_{ionosonde}^i\right)^2} \quad (18)$$

$$Bias = \frac{1}{M}\sum_{i=1}^{M}\left(N_R^i - N_{ionosonde}^i\right) \quad (19)$$

$$R = 1 - \frac{\sum_{i=1}^{M}\left(N_R^i - N_{ionosonde}^i\right)^2}{\sum_{i=1}^{M}\left(\overline{N} - N_{ionosonde}^i\right)^2} \quad (20)$$

where N_R is the reconstructed value of electron density, $N_{ionosonde}$ is the observed value of electron density from ionosondee, $\overline{N}$is the mean value of electron density and $M$is the number of sample elements. If the value of the RMSE and bias is close to zero, it indicates the high accuracy of the model. The correlation coefficient expresses the correlation between two variables. In other words, this index expresses the changes of two variables relative to each other. The value of this coefficient is in the range [0, 1]. If the correlation coefficient of two variables is close to one, it indicates their high correlation. Zero correlation coefficient indicates no correlation between two variables.

Results and Discussion

In the training part of all 3 methods (RMTNN, MRMTNN, and ITNN), input space included 4 observations which are used to train and obtain the variations of the ionospheric electron density. Therefore, the predicted N is a function of 4 inputs and can be simply expressed mathematically according to the following expression [24]:

$$N_R = f(latitude \quad longitude \quad altitude \quad time) \quad (21)$$

Figure 3 illustrates schematic diagrams of the data flow for pixel-based ionospheric tomography by a neural network with BP and PSO training algorithm.

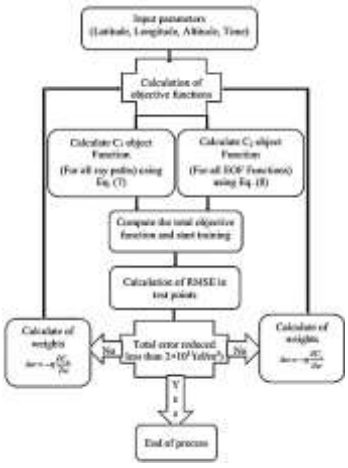

Fig. 3. Schematic diagram of the data flow for pixel-based ionospheric tomography using neural network training with BP algorithm.

It should be mentioned that in the case of using the PSO algorithm, in Figure (3), instead of updating the weights, the parameters of the PSO algorithm are updated. It should be noted that after extensive testing, the 4-18-1 structure was selected as the optimum structure for all 3 methods. In this structure, 4 represents the number of model inputs, 18 represents the number of hidden layer neurons, and number 1 represents the model output. Figure 4 illustrates the error curve of 3 methods in terms of RMSE at the testing step.

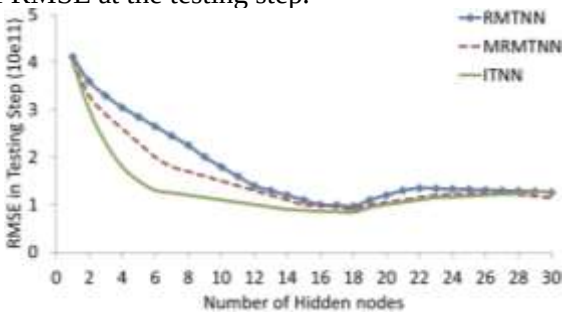

Fig. 4. Error curve of 3 methods in terms of RMSE at the testing step.

According to Figure 4, all 3 methods converge to the lowest error with 18 neurons in the hidden layer. The performance of the proposed methods (RMTNN, MRMTNN, and ITNN) is compared in terms of RMSE (10^{11} ele./m^3) in the testing step and time of convergence (second) to the optimal solution. Table 1 shows this comparison. It should be noted that all model computations were done in a computer system with similar hardware and software.

Table 1. Comparison of RMSE for the testing step of RMTNN, MR,MTNN and ITNN methods for periods of 354 to 363, 44 to 53, and 67 to 76.

DOY	RMSE in the testing step (10^{11} ele./m^3)		
	RMTNN	MRMTNN	ITNN
354 to 363	0.97	0.91	0.84
44 to 53	1.42	1.21	0.95
67 to 76	2.14	1.77	1.38

Table 2. Comparison of times of convergence of RMTNN, MR, MTN,N, and ITNN methods for periods of 354 to 363, 44 to 5,3, and 67 to 76.

DOY	Time of convergence (second)		
	RMTNN	MRMTNN	ITNN
354 to 363	529	479	421
44 to 53	580	524	483
67 to 76	634	597	533

Using the results presented in Tables 1 and 2, the difference between the methods becomes apparent. The time of convergence to the optimal solution and RMSE for the testing step in the ITNN method is less than the MRMTNN and

RMTNN methods. The time of convergence to the optimal solution is considerably reduced in ITNN method with respect to RMTNN method (original method). This result reflects the fact that using WNN with PSO training algorithm (ITNN method) computational speed is increased. Another very important point in Tables 1 and 2 is that the RMSE in the testing step at all 3 methods has increased in a period of 67 to 76. In other words, in periods of high geomagnetic activity, all 3 methods displayed results with lower accuracy compared to the quiet and medium conditions.

Validation, verification, and reconstruction of electron density

After optimization of neural networks (SANN and WNN) in terms of network structure (4-18-1), RMSE and time of convergence to the optimal solution at the testing step, it is possible to validate of accuracy of results for all 3 methods. For this purpose, in the geographical positions of 4 ionosondee stations, electron density was reconstructed using 3 methods and compared with the corresponding ionosondee electron density. This comparison has been done at a height of 100 to 600 km with 50 km altitude intervals. The RMSE and bias statistical indicators are used to describe the error values. It should be noted that RMSE is often used to verify the reliability of the proposed method. All computations were performed for 3 different periods of geomagnetic activities. Tables 3, 4, 5 and 6 represent computations in 4 ionosondee stations (DOUR, JULI, PRUH and WARS).

Table 3. Averaged RMSE (10^{11} ele./m^3) and bias (10^{11} ele./m^3) in selected heights (100 to 600 km with 50 km height interval) over DOUR ionosondee station

		354 to 363	44 to 53	67 to 76
RMTNN	RMSE	1.18	1.32	1.61
	Bias	1.02	1.18	1.44
MRMTNN	RMSE	0.92	1.24	1.49
	Bias	0.81	1.03	1.21
ITNN	RMSE	0.52	0.89	1.22
	Bias	0.43	0.72	0.97

The results in Table 3 demonstrate that the RMSE and bias of the ITNN method are less than the other two methods. It means that by using WNN with the PSO training algorithm, the accuracy of the method is considerably increased. On the other hand, in comparison with the original method (RMTNN) proposed by [9], the ITNN method is improved electron density reconstruction. It should be noted that even the MRMTNN method is also more accurate than the RMTNN method. In other words, by varying the SANN to WNN, results improved. Another important point is that all 3 methods have a lower accuracy during high geomagnetic activity. Table 4 demonstrates the results of RMSE and bias analysis in the JULI ionosondee station.

Table 4. Averaged RMSE (10^{11} ele./m^3) and bias (10^{11} ele./m^3) in selected heights (100 to 600 km with 50 km height interval) over JULI ionosondee station

		354 to 363	44 to 53	67 to 76
RMTNN	RMSE	1.42	1.84	2.03
	Bias	1.21	1.52	1.93
MRMTNN	RMSE	1.23	1.42	1.79
	Bias	1.12	1.26	1.44
ITNN	RMSE	0.88	1.19	1.46
	Bias	0.71	1.11	1.30

The obtained results in this station represent the superiority of the ITNN method with respect to the other two methods. Results for the PRUH ionosondee station are shown in Table 5.

Table 5. Averaged RMSE (10^{11} ele./m^3) and bias (10^{11} ele./m^3) in selected heights (100 to 600 km with 50 km height interval) over PRUH ionosondee station

		354 to 363	44 to 53	67 to 76
RMTNN	RMSE	1.09	1.27	1.46
	Bias	0.88	1.09	1.27
MRMTNN	RMSE	0.79	1.06	1.21
	Bias	0.55	0.89	0.94
ITNN	RMSE	0.54	0.81	1.18
	Bias	0.47	0.72	0.93

In PRUH ionosondee station, the obtained results from ITNN method is accurate than the RMTNN and MRMTNN methods. In quiet and medium conditions, the superiority of ITNN method is much clearer than the stormy conditions.

Table 6. Averaged RMSE (10^{11} ele./m^3) and bias (10^{11} ele./m^3) in selected heights (100 to 600 km with 50 km height interval) over WARS ionosondee station

		354 to 363	44 to 53	67 to 76
RMTNN	RMSE	1.14	1.32	1.58
	Bias	0.91	1.13	1.34
MRMTNN	RMSE	0.97	1.21	1.43
	Bias	0.75	1.03	1.11
ITNN	RMSE	0.79	0.98	1.18
	Bias	0.66	0.94	1.02

Another important point that can be interpreted from the above tables is that the RMSE of the models in the JULI ionosondee station is more than the other three stations. Referring to Figure 1, it can be seen that this ionosondee station is farther from the GPS station than other ionosondee stations. This factor has reduced the accuracy of modeling in this station. For analysis of the accuracy of the methods in ionospheric electron density reconstruction, results were compared with ionosondee direct measurements. Figure 5 indicates the scatter plot for RMTNN, MRMTNN, and ITNN electron density with corresponding electron density from the ionosondee at 3 periods with lines of best fit shown for all cases.

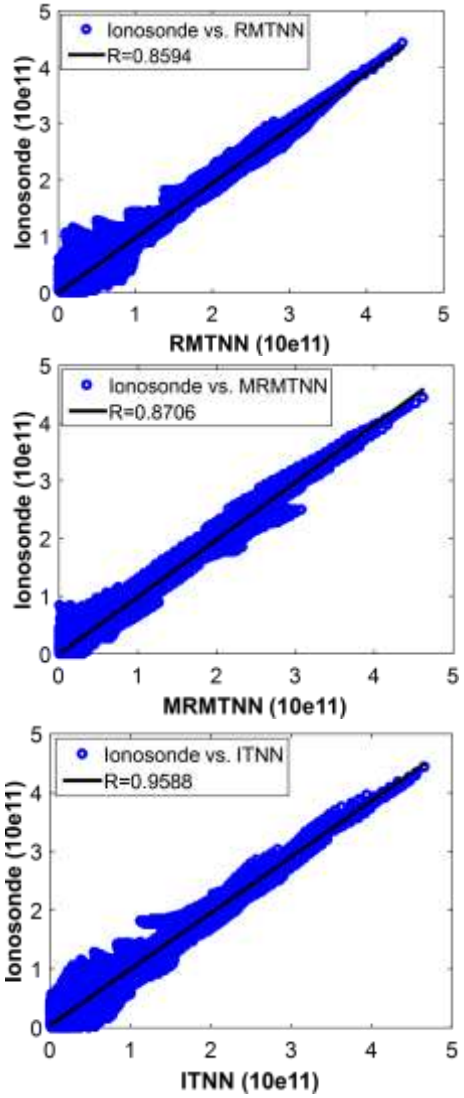

Fig. 5. Scatter plots for ionosondee electron density (10^{11} ele./m^3) in vertical axes and corresponding reconstructed electron density (10^{11} ele./m^3) in horizontal axes using RMTNN (top), MRMTNN (middle), and ITNN (bottom) in 3 periods 354 to 363, 44 to 53 and 67 to 76.

Using Figure 5, it is visible that the ITNN method is highly correlated to ionosondee measurements with a correlation coefficient (R) of 0.9588. The values of the correlation coefficient between MRMTNN and RMTNN with ionosondee measurements are 0.8706 and 0.8594, respectively. These results again indicate that the original ionospheric reconstruction method (RMTNN) is improved.

After assessing the accuracy of the proposed methods, it is possible to draw profiles of time-dependent ionosphere electron density profiles. The results of this analysis for the ITNN method are shown in Figures 6, 7, and 8. In these figures, reconstructed electron density profiles using ITNN were compared with the corresponding ionosondee profiles and NeQuick empirical ionosphere model electron density. All these comparisons have been conducted for the height of 350 km at 3 periods of geomagnetic activity (354 to 363, 44 to 53 and 67 to 76). The NeQuick is a quick-run ionospheric electron density model particularly designed for trans-ionospheric propagation applications. The NeQuick gives the electron density for positions in the ionosphere with height, geocentric latitude, and geocentric longitude as coordinates on a spherical earth. The model values depend on solar activity (given by monthly-mean sunspot number R12 or 10.7 cm solar radio flux F10.7) season (month) and time (Universal Time).

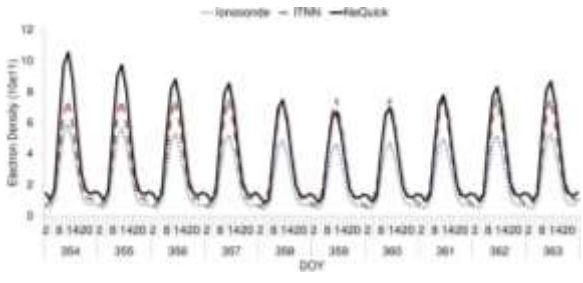

Fig. 6. Comparison of daily variation of electron density (10^{11} ele./m^3) at 10 days (354 to 363) for ITNN, ionosondee, and NeQuick models over PRUH ionosondee station at the altitude of 350 km.

According to the results of Figure 6, ITNN reconstructed electron densities on most days are very close to the ionosondee electron density profiles. It should be noted that the NeQuick model has shown better results in some days (358, 359 and 360). The greatest value of the difference

between the ionosondee and ITNN electron density ($dN=N_{ionosondee} - N_{ITNN}$) has happened on the DOY of 360. According to Figure 2, DOY of 360 has high geomagnetic activity with respect to the other days in this period. Figure 7 represents the electron density profiles for the period of 44 to 53.

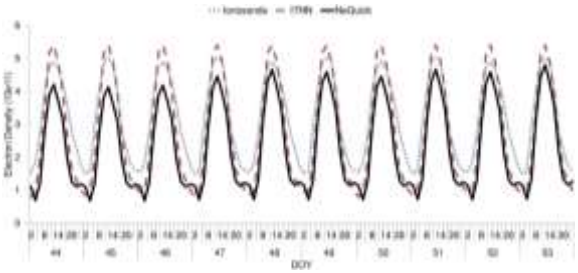

Fig. 7. Comparison of daily variation of electron density (10^{11} ele./m^3) at 10 days (44 to 53) for ITNN, ionosondee, and NeQuick models over PRUH ionosondee station at an altitude of 350 km.

The results in Figure 7 show the high accuracy of the ITNN method. In all days, the ITNN model reconstructed electron density better than the NeQuick model. The results of the time-dependent electron density profile for the period of 67 to 76 are shown in Figure 8.

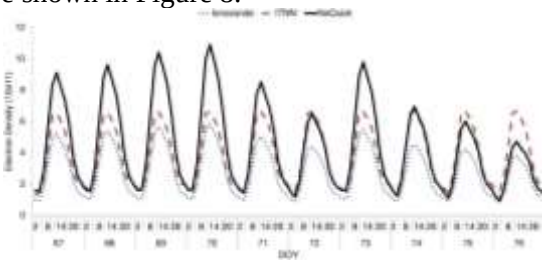

Fig. 8. Comparison of daily variation of electron density (10^{11} ele./m^3) at 10 days (67 to 76) for ITNN, ionosondee and NeQuick models over PRUH ionosondee station at an altitude of 350 km.

According to Figure 8, on some days (72, 75, and 76), the NeQuick model has higher accuracy with respect to the ITNN method. In other words, these days, the value of $dN=N_{ionosondee} - N_{NeQuick}$ is less than the value of $dN=N_{ionosondee} - N_{ITNN.}$ Using these Figures (6, 7 and 8), it is obvious that the peak of electron density occurs between 08:00 to 10:00 UT and also temporal variation of ionospheric electron density can be seen clearly.

Discussion and conclusion

In this paper, voxel-based ionospheric tomography is solved using Artificial Neural Networks (ANNs). Three methods of ionospheric reconstruction were compared and evaluated. Residual Minimization Training Neural Network (RMTNN), Modified RMTNN (MRMTNN) and Ionospheric Tomography based on the Neural Network (ITNN) were studied in this paper. In the RMTNN method, Standard ANN (SANN) with a Back-Propagation (BP) training algorithm is used to reconstruct the ionosphere. Wavelet Neural Network (WNN) is used as a base network in the MRMTNN method. Also, the BP algorithm is used to train the network. In the ITNN method, instead of the BP algorithm and speeding up the convergence to the optimal solution, the Particle Swarm Optimization (PSO) algorithm is used. All 3 methods were evaluated using IGS data in central Europe. To evaluate the accuracy of the proposed methods, 4 ionosondee stations were used. Three time periods (354 to 363, 44 to 53, and 67 to 76) with different geomagnetic activity indexes were used to evaluate the effectiveness of the models in different conditions. The time of convergence to the optimal solution and RMSE in the testing step were compared in the proposed methods. These two indexes in the ITNN method were less than the MRMTNN and ITNN methods. After the optimization of neural networks (SANN and WNN) in terms of RMSE and convergence speed, the accuracy of the proposed methods was investigated in ionosondee stations. RMSE and bias values for all 3 methods were computed. The obtained results represent that the ITNN method was superior to the other two methods. It means that by using WNN with the PSO training algorithm, the accuracy of the method considerably increased. Also the scatter plot for ionosondee electron density with corresponding electron density predictions from three methods computed. In this case, the ionosondee electron density is highly correlated to ITNN with a correlation coefficient (R) of 0.9588 and the lowest correlated with a correlation coefficient of 0.8594 in RMTNN.

The results of this paper have shown that the ITNN model has a high accuracy in modeling the spatio-temporal variations of ionospheric electron density. Also, this model is more accurate than the empirical ionosphere model in the period of high geomagnetic activities. The ITNN model has the capability of local modeling of electron density and provides the density value with high accuracy by entering the latitude, longitude, altitude, and time parameters. Therefore, it can be an alternative to mathematical and empirical ionosphere models.

The presented new model has the limitation of not considering effective solar and geomagnetic parameters in the modeling step as input parameters of the model. Therefore, in order to continue the research, solar and geomagnetic parameters can be considered as input in the modeling step. Also, the number of used stations can be reduced and the accuracy of spatial modeling can be evaluated more accurately.

Acknowledgments

RINEX observation files were downloaded from the Crustal Dynamics Data Information System (CDDIS) as a global data center of IGS (ftp://cddis.gsfc.nasa.gov/pub/gps/data/daily). We acknowledge the CDDIS center for making RINEX observation data freely available. Also, Ionosondee data can be obtained http://car.uml.edu/common/DIDBStationList. We express our thanks to reviewers for their helpful comments and suggestions which improved the quality of this paper.

Conflicts of Interest

The authors of this paper declared no conflict of interest regarding the authorship or publication of this article.

References

[1] J. R., Austen, S.J., Franke, C. H., Liu, "Ionospheric imaging using computerized tomography". Radio Sci., vol. 23, pp. 299–307, 1988.

[2] V.E., Kunitsyn, I.A., Nesterov, A. M., Padokhin, U. S., Tumanova, "Ionospheric radio tomography based on the GPS/GLONASS navigation systems". J Commun Technol Electron, vol. 56, pp. 1269–1281, 2011.

[3] D., Pokhotelov, P., Jayachandran, C. N., Mitchell, J. W., MacDougall, M. H., Denton, "GPS tomography in the polar cap: comparison with ionosondees and in situ spacecraft data". GPS Solut, vol. 15, pp. 79–87, 2011.

[4] D. B., Wen, Y., Wang, R., Norman, "A new two-step algorithm for ionospheric tomography solution," GPS Solut., vol. 16, pp. 89-94, 2012.

[5] M.M.J.L., Van de Kamp, "Medium-scale 4-D ionospheric tomography using a dense GPS network". Ann Geophys., vol. 31, pp. 75-89, 2013.

[6] M.R., Ghaffari Razin, "Development and analysis of 3D ionosphere modeling using base functions and GPS data over Iran". Acta Geod Geophys, vol. 51, pp. 95-111, 2015.

[7] M.R., Ghaffari Razin, B., Voosoghi, "Regional ionosphere modeling using spherical cap harmonics and empirical orthogonal functions over Iran". Acta Geod. Geophys., vol. 52, pp. 19-33, 2016.

[8] A., Yilmaz, K.E., Akdogan, M., Gurun, "Regional TEC mapping using neural networks". Radio Sci, vol. 44, pp. 1-16 , 2009.

[9] X.F., Ma, T., Maruyama, G., Ma, T., Takeda, "Three dimensional ionospheric tomography using observation data of GPS ground receivers and ionosondee by neural network". J. Geophys. Res., vol. 110, pp. 1-12, 2005.

[10] S., Hirooka, K., Hattori, T., Takeda, "Numerical validations of neural-network-based ionospheric tomography for disturbed ionospheric conditions and sparse data". Radio Sci., vol. 46, 2011.

[11] M. R., Ghaffari Razin, B., Voosoghi, "Regional application of multi-layer artificial neural networks in 3D ionosphere tomography". Adv Space Res, vol. 58 pp. 339–348, 2016.

[12] ftp://cddis.gsfc.nasa.gov/pub/gps/data/daily.

[13] http://car.uml.edu/common/DIDBStationList.

[14] L., Ciraolo, F., Azpilicueta, C., Brunini, A., Meza, S. M., Radicella, "Calibration errors on experimental Slant Total Electron Content (TEC) determined with GPS". Journal of Geodesy, vol. 81, pp:111–120, 2007.

[15] A., Liaqat, M., Fukuhara, T., Takeda, "optimal estimation of parameter of dynamical system by neural network collocation method". Comput. Phys. Commun, vol. 150, pp. 215–234, 2003.

[16] G., Seeber, "Satellite Geodesy, Foundations, Methods and Application", Walter de Gruyter, Berlin and New York, 531.

[17] A., Quarteroni, R., Sacco, F., Saleri, "Numerical Mathematics, 37, Texts in Applied Mathematics", Springer Berlin Heidelberg, Heidelberg, Germany, 2007.

[18] A., Alexandridis, A., Zapranis, "Wavelet neural networks: A practical guide". Neural Networks, vol. 42, pp, 1–27, 2013.

[19] Y., Becerikli, Y., Oysal, A. F., Konar, "On a dynamic wavelet network and its modeling application". In Lecture Notes in Computer Science, vol, 2714, pp. 710–718, 2003.

[20] S. A., Billings, H. L., Wei, "A new class of wavelet networks for nonlinear system identification". IEEE Transactions on Neural Networks, vol. 16, pp. 862–874, 2005.

[21] Y., Oussar, G., Dreyfus, "Initialization by selection for wavelet network training". Neurocomputing, vol. 34, pp. 131–143, 2000.

[22] L., Xu, D. W. C., Ho, "A basis selection algorithm for wavelet neural networks". Neurocomputing, vol. 48, pp. 681–689, 2002.

[23] Q., Zhang, A., Benveniste, "Wavelet Networks". IEEE Trans. Neural Networks, vol. 3, pp.889–898, 1992.

[24] M. R., Ghaffari Razin, B., Voosoghi, " Wavelet neural networks using particle swarm optimization training in modeling regional ionospheric total electron content". Journal of Atmospheric and Solar-Terrestrial Physics, vol. 149, pp. 21-30, 2016.

[25] M. R., Ghaffari Razin, B., Voosoghi, " Modeling of ionosphere time series using wavelet neural networks (case study: NW of Iran)". Advances in Space Research, vol. 58, pp. 74-83, 2016.

HOW TO CITE THIS ARTICLE:
SeyyedReza Ghaffari Razin**,** Reza Davari Majd, Behzad Voosoghi, Navid Hooshangi "*Ionospheric electron density reconstruction over central Europe using neural networks: A comparative study*", Journal of Aerospace Science and Technology, Vol 17, No1,2024, pp, 23-33
DOI: doi.org/10.22034/jast.2023.187660.1020
URL: https://jast.ias.ir/article_181480.html